

1 **TITLE**

2 PELP1/SRC-3-dependent regulation of metabolic kinases drives therapy resistant ER+ breast  
3 cancer

4

5 **AUTHORS**

6 Thu H. Truong<sup>1</sup>, Elizabeth A. Benner<sup>1</sup>, Kyla M. Hagen<sup>1</sup>, Nuri A. Temiz<sup>1,4</sup>, Carlos Perez Kerkvliet<sup>1</sup>,  
7 Ying Wang<sup>1</sup>, Emilio Cortes-Sanchez<sup>6,7,8</sup>, Chieh-Hsiang Yang<sup>6,7,8</sup>, Thomas Pengo<sup>5</sup>, Katrin P.  
8 Guillen<sup>6,8</sup>, Bryan E. Welm<sup>6,7,8</sup>, Sucheta Telang<sup>9</sup>, \*Carol A. Lange<sup>1,2,3</sup>, and \*Julie H. Ostrander<sup>1,2</sup>

9 \* co-senior authors

10

11 **AFFILIATIONS**

12 <sup>1</sup> Masonic Cancer Center, <sup>2</sup> Department of Medicine (Division of Hematology, Oncology, and  
13 Transplantation), <sup>3</sup>Department of Pharmacology, <sup>4</sup> Institute for Health Informatics, and <sup>5</sup>University  
14 of Minnesota Informatics Institute, University of Minnesota, Minneapolis MN 55455 USA

15 <sup>6</sup>Department of Oncological Sciences, <sup>7</sup>Department of Surgery, and <sup>8</sup>Huntsman Cancer Institute,  
16 University of Utah, Salt Lake City UT 84112,

17 <sup>9</sup>James Graham Brown Cancer Center, Department of Medicine (Division of Medical Oncology  
18 and Hematology), University of Louisville, Louisville KY 40202 USA

19

20 **RUNNING TITLE**

21 PELP1/SRC-3 regulate metabolic kinases in ER+ breast cancer

22

23 **KEYWORDS**

24 PELP1, SRC-3, cancer stem cells

25

26 **FINANCIAL SUPPORT**

27 This work was supported by NIH grants R01 CA236948 (JHO, CAL), F32 CA210340 (THT), T32  
28 HL007741 (THT), and U54 CA224076 (BEW), ACS Institutional Research Grant #124166-IRG-  
29 58-001-52-IRG5 (JHO), University of Minnesota Masonic Cancer Center (CAL, JHO), the Tickle  
30 Family Land Grant Endowed Chair in Breast Cancer Research (CAL), National Center for  
31 Advancing Translational Sciences of the NIH Award UL1TR000114 (JHO), and Department of  
32 Defense W81XWH-14-1-0417 (BEW).

33

34

35 **CORRESPONDING AUTHORS**

36 Julie H. Ostrander

37 [hans1354@umn.edu](mailto:hans1354@umn.edu) (email), 612-625-1996 (phone)

38 University of Minnesota Masonic Cancer Center

39 Cancer and Cardiovascular Research Building

40 Delivery Code 2812

41 2231 6<sup>th</sup> St SE, Minneapolis MN 55455, USA

42

43 Carol A. Lange

44 [lange047@umn.edu](mailto:lange047@umn.edu) (email), 612-626-0621 (phone)

45 University of Minnesota Masonic Cancer Center

46 Cancer and Cardiovascular Research Building

47 Delivery Code 2812

48 2231 6<sup>th</sup> St SE, Minneapolis MN 55455, USA

49

50 **CONFLICT OF INTEREST**

51 Carol A. Lange is a Scientific Advisory Board Member for Context Therapeutics, Inc. The

52 remaining authors have nothing to disclose.

53

54 **WORD COUNT:** 5,814

55 **FIGURES:** 7

56 **TABLES:** 0

57

58

59

60

61

62

63

64

65

66

67

68

69 **ABSTRACT**

70 Recurrence of metastatic breast cancer stemming from acquired endocrine and chemotherapy  
71 resistance remains a health burden for women with luminal (ER+) breast cancer. Disseminated  
72 ER+ tumor cells can remain viable but quiescent for years to decades. Contributing factors to  
73 metastatic spread include the maintenance and expansion of breast cancer stem cells (CSCs).  
74 Breast CSCs frequently exist as a minority population in therapy resistant tumors. In this study,  
75 we show that cytoplasmic complexes composed of steroid receptor (SR) co-activators, PELP1  
76 and SRC-3, modulate breast CSC expansion through upregulation of the HIF-activated metabolic  
77 target genes *PFKFB3* and *PFKFB4*. Seahorse metabolic assays demonstrated that cytoplasmic  
78 PELP1 influences cellular metabolism by increasing both glycolysis and mitochondrial respiration.  
79 PELP1 interacts with PFKFB3 and PFKFB4 proteins, and inhibition of PFKFB3 and PFKFB4  
80 kinase activity blocks PELP1-induced tumorspheres and protein-protein interactions with SRC-3.  
81 PFKFB4 knockdown inhibited *in vivo* emergence of circulating tumor cell (CTC) populations in  
82 mammary intraductal (MIND) models. Application of PFKFB inhibitors in combination with ER  
83 targeted therapies blocked tumorsphere formation in multiple models of advanced breast cancer,  
84 including tamoxifen (TamR) and paclitaxel (TaxR) resistant models and ER+ patient-derived  
85 organoids (PDxO). Together, our data suggest that PELP1, SRC-3, and PFKFBs cooperate to  
86 drive ER+ tumor cell populations that include CSCs and CTCs.

87 **Significance:** Identifying non-ER pharmacological targets offers a useful approach to blocking  
88 metastatic escape from standard of care ER/estrogen (E2)-targeted strategies to overcome  
89 endocrine and chemotherapy resistance.

90

91

92 **INTRODUCTION**

93 Metastatic recurrence is an incurable but common complication of ER+ breast cancer. Treatment  
94 of metastatic breast cancer typically results in endocrine resistance, and chemotherapy is largely  
95 ineffective in advanced disease. Altered signaling pathways drive therapy resistance and offer  
96 potential targets for metastatic ER+ breast cancer. PELP1 (proline, glutamic acid, leucine-rich  
97 protein 1) and SRC-3 (steroid receptor [SR] co-activator-3) have independently been shown to  
98 drive endocrine resistance. PELP1 and SRC-3 are both SR co-activators involved in normal  
99 development and cancer (1,2). Increased PELP1 expression is associated with higher tumor  
100 grade, tumor proliferation, and decreased breast cancer-specific survival (3,4). PELP1 is primarily  
101 nuclear in normal breast tissue; however, altered cytoplasmic PELP1 localization is observed in  
102 40-58% of PELP1+ breast tumors (5). Analysis of breast tumor samples revealed that patients

103 with high cytoplasmic PELP1 levels were less likely to respond to tamoxifen (tam) (4). Similarly,  
104 SRC-3 mRNA and protein overexpression are correlated with higher tumor grade and decreased  
105 overall and disease-free survival (6). SRC-3 overexpression is also linked to tam resistance in  
106 breast cancer models and human breast tumors (7,8). Both PELP1 and SRC-3 have essential  
107 nuclear functions, but also dynamically shuttle to the cytoplasm where they associate with  
108 signaling molecules and act as scaffolds for growth factor or SR pathways. These SR co-  
109 activators have emerged as promising targets in ER+ breast cancer and as potential mediators  
110 of therapy resistance.

111  
112 Cancer stem cells (CSCs) are poorly proliferative and frequently exist as a minority sub-population  
113 of cells that drive therapy resistance and metastasis (9). In contrast to non-CSCs, breast CSCs  
114 form colonies in serum-free suspension culture (i.e. tumorspheres), express stem cell markers  
115 (e.g. ALDH+ or CD44<sup>hi</sup>/CD24<sup>lo</sup>), exhibit enhanced resistance to chemo and endocrine therapies,  
116 and express markers of epithelial to mesenchymal transition (EMT). The ability to survive and  
117 self-renew following treatment allows CSCs to evade standard chemo and endocrine therapies  
118 aimed at rapidly dividing cancer cells and to drive metastatic tumor growth.

119  
120 Growing evidence has implicated SR co-activators as mediators of CSC self-renewal. For  
121 example, SRC-3 drives CSC formation and tumor outgrowth in breast cancer models. Treatment  
122 with SI-2, an SRC-3 inhibitor, decreased SRC-3-induced CSC formation in breast cancer cell and  
123 xenograft models (10). Our laboratory reported that cytoplasmic complexes composed of PELP1  
124 and SRC-3 mediate breast CSC expansion (11). Targeting SRC-3 using shRNA or  
125 pharmacological inhibitors (i.e. SI-2) abrogated PELP1/SRC-3 complex formation, PELP1-  
126 induced tumorspheres, and expression of PELP1 target genes that promote cancer cell survival.  
127 These studies imply that inhibiting PELP1 and its binding partners may provide a way to target  
128 the breast CSC population in order to improve patient outcomes.

129  
130 Herein we sought to identify the molecular mechanisms that contribute to PELP1-driven CSC  
131 survival and self-renewal in ER+ breast cancer. Using endocrine and chemotherapy resistant  
132 breast cancer models, our findings suggest that PELP1/SRC-3 complexes modulate the CSC  
133 compartment through gene programs associated with metabolic adaptation. In contrast to current  
134 therapies that fail to adequately target slow-growing breast CSCs, our studies reveal therapy  
135 combinations that inhibit cooperating signaling cascades, while simultaneously targeting ER. By

136 targeting CSCs directly, this approach promises to significantly improve the lives of patients with  
137 recurrent ER+ breast cancer.

138

139

140 **MATERIALS AND METHODS**

141 **Cell Culture.** STR authentication was performed by ATCC (October 2018). MCF-7 PELP1 and  
142 J110 cells were cultured as described (11). MCF-7 (12) and T47D TamR (13) cells were cultured  
143 in 100 nM tamoxifen. MCF-7 TaxR (14) cells were cultured in 2  $\mu$ M Taxol. For 3D (tumorsphere)  
144 conditions, cells were cultured as described (11).

145

146 **Patient-Derived Organoids (PDxO).** PDxOs (HCl-003, -011, -017) were cultured in Advanced  
147 DMEM/F12 (Thermo Fisher) containing 5% FBS, 1X HEPES, 1X GlutaMax, 50  $\mu$ g/ml Gentamicin  
148 (Genesee), 1  $\mu$ g/ml hydrocortisone, 10 ng/ml EGF, and supplemented with 10  $\mu$ M Y-27632  
149 (Selleckchem), 100 ng/ml FGF2 (PeproTech), and 1 mM N-acetyl cysteine (Sigma). PDxOs were  
150 embedded into Matrigel (growth factor reduced; Corning) using the hanging drop method into 6-  
151 well plates and passaged every ~14-18 days.

152

153 **Synergy Screens.** PDxOs were grown as described above in 384-well plates: Prior to assay,  
154 PDxOs were cultured in PDxO media containing charcoal stripped FBS and allowed to incubate  
155 overnight. PDxOs were disbursed with Dispase and re-seeded in PDxO media on 384-well plates  
156 coated with Matrigel. Following 24h after seeding, plates were dosed with SI-2 (0-2  $\mu$ M), 5MPN  
157 (0-50  $\mu$ M), and tam (0-10  $\mu$ M) using a robotic assisted pipette (ViaFlo). On Day 6 post-treatment,  
158 a Cell Titer Glo 3D assay (Promega) was performed per manufacturer's instructions.  
159 Luminescence readings were measured using an Envision Spectrophotometer. Fold changes  
160 were calculated using Day 0 baseline readings. % survival was calculated for each well, and ZIP  
161 synergy model (15) were run to determine synergy scores with the R package synergy finder (16).  
162 Independent drug response was calculated using the four- parameter logistic model (4-PL). 3  
163 biological replicates, each one consisting of 4 technical replicates per dosing, was performed.

164

165 **Mammary Intraductal (MIND) Model.** Intraductal injections of single cells were performed as  
166 described (17,18). Seven-week old female NSG mice (#005557) were purchased from Jackson  
167 Laboratory. Five mice/group were injected with  $5 \times 10^4$  cells into each nipple of the 4<sup>th</sup> inguinal  
168 glands with the indicated breast cancer cell line. Mammary glands were harvested 8 weeks after

169 injection, fixed in 4% PFA, and processed for H&E staining. H&E sections were analyzed using  
170 ImageJ or Q-path to quantitate the total mammary gland area (%) that contained tumor cells.

171  
172 **Statistical Analysis.** Data were tested for normal distribution using Shapiro-Wilks normality test  
173 and homogeneity of variances using Bartlett's Test. Once data met these two requirements,  
174 statistical analyses were performed using one-way or two-way ANOVA in conjunction with Tukey  
175 multiple comparison test for means between more than two groups or Student *t* test for means  
176 between two groups, where significance was determined with 95% confidence. For the MIND  
177 study with four groups defined by two factors (cyto PELP1 vs. WT PELP1, and shPFKFB4 vs.  
178 shGFP), a regression model identified a significant interaction due to shPFKFB4 at an alpha level  
179 of 0.1 (p=0.084).

180

181

## 182 **RESULTS**

### 183 **Cytoplasmic PELP1 promotes CSCs and HIF-regulated gene expression**

184 Breast CSCs represent a minority of the total cell population (1-5%) (19), making it difficult to  
185 detect CSC-specific changes in bulk tumor populations. We therefore measured breast CSC  
186 frequency by comparing ALDH activity (**Figure 1A, Supplementary Figure 1**) and CD44<sup>hi</sup>/CD24<sup>lo</sup>  
187 ratios (**Figure 1B, Supplementary Figure 2**) in MCF-7 cells stably expressing LXS (vector  
188 control), WT PELP1, or cytoplasmic (cyto) PELP1 cultured in either 2D (adherent) or 3D  
189 (tumorsphere) conditions. Relative to 2D, 3D conditions increased breast CSC markers in MCF-  
190 7 cells expressing LXS, WT PELP1, or cyto PELP1 (**Figure 1A, 1B**). In 2D conditions, cyto  
191 PELP1 expressing cells had no significant changes in ALDH activity when compared to LXS or  
192 WT PELP1; however, when the same models were cultured in 3D conditions, ALDH activity was  
193 significantly increased in cells expressing cyto PELP1 (12.0%  $\pm$  2.9) compared to LXS (6.6%  $\pm$   
194 0.67,  $p$  = 0.023) and WT PELP1 (2.6%  $\pm$  0.76,  $p$  = 0.0015). In 2D conditions, CD44<sup>hi</sup>/CD24<sup>lo</sup>  
195 populations were increased in cyto PELP1 expressing cells (13.0%  $\pm$  0.49) compared to LXS  
196 (2.6%  $\pm$  0.042,  $p$  < 0.0001) or WT PELP1 (1.2%  $\pm$  0.19,  $p$  < 0.0001), and this trend was enhanced  
197 in 3D conditions (cyto PELP1, 19.4%  $\pm$  1.4; LXS, 9.0%  $\pm$  1.1,  $p$  = 0.0045; WT PELP1, 2.3%  $\pm$   
198 0.18,  $p$  = 0.0011). WT PELP1 displayed lower ALDH activity and CD44<sup>hi</sup>/CD24<sup>lo</sup> ratios relative to  
199 LXS controls, suggesting that nuclear PELP1 limits CSC behavior. These results indicate that  
200 both 3D culture and cyto PELP1 expression independently increase CSC expansion in MCF-7  
201 cell models.

202

203 We performed RNA-seq on MCF-7 PELP1 models grown as 3D tumorspheres and compared  
204 these data to studies conducted in 2D culture (11) to identify candidate genes and pathways  
205 differentially regulated in cyto PELP1 expressing cells. Comparison of 3D versus 2D conditions  
206 identified 206 upregulated and 114 downregulated genes similarly regulated by >2-fold in all cell  
207 lines (LXSN, WT PELP1, cyto PELP1) (**Figure 1C, Supplementary Figure 3**). Ingenuity Pathway  
208 Analysis (IPA) of these 320 genes revealed activation of estrogen, growth factor, cytokine, and  
209 NF- $\kappa$ B pathways (**Supplementary Table 1**). Significantly activated and inhibited “Diseases and  
210 Functions” are summarized in **Supplementary Table 2**. 3D to 2D comparison in cyto PELP1  
211 expressing cells identified 173 differentially expressed genes (93 upregulated, 80 downregulated)  
212 compared to LXSN or WT PELP1 (**Figure 1C, Supplementary Figure 4**). These 173 genes were  
213 analyzed with IPA to identify cyto PELP1-specific pathways (**Figure 1D**), biological functions, or  
214 disease states (**Figure 1E**), and predicted increased HIF activation, estradiol, ATF4, and  
215 glycolytic-mediated pathways. We created representative heatmaps to illustrate 3D-specific  
216 regulation in upstream regulator analysis associated with HIF and ATF4 pathway activation (>2-  
217 fold; **Figure 1F**) and generated a cyto PELP1 upregulated gene signature (**Supplementary Table**  
218 **3**). Volcano plots of differentially regulated genes are shown in **Figure 1G**; red dots indicate genes  
219 in the cyto PELP1 signature. We then used the cyto PELP1 upregulated gene signature to query  
220 the METABRIC breast cancer database. Higher expression of this gene signature was associated  
221 with lower overall survival (OS) in the METABRIC cohort (hazard ratio = 1.485, p < 0.0001, **Figure**  
222 **1H**). We tested this on the ER+ only subtype within the METABRIC cohort and found similar  
223 results (hazard ratio = 1.483, p < 0.0001, **Figure 1I**). A similar query of the TCGA database  
224 revealed no significant differences in OS (**Supplementary Figure 5**). Taken together, these data  
225 identify genes involved in cyto PELP1-mediated pathways that promote CSCs, including those  
226 associated with HIF-activated and glycolytic pathways.

227

## 228 **Cytoplasmic PELP1 drives metabolic plasticity**

229 Given the strong activation of HIF and metabolic pathways detected in the RNA-seq analysis, we  
230 used qPCR to test HIF-activated target genes. HIF activates the *PFKFB* family, which are  
231 metabolic bi-functional kinase/phosphatases (20). We found that mRNA levels of *EPAS1* (i.e.  
232 HIF2 $\alpha$ ), *PFKFB3*, and *PFKFB4* were upregulated in cells expressing cyto PELP1 relative to LXSN  
233 or WT PELP1 in 3D, but not 2D conditions (**Figure 2A**). Additional validation of HIF-activated  
234 metabolic and stem cell genes include *NDRG1* and *SOX9* (**Figure 2A**). Given the central role of  
235 HIF pathways in metabolism (21), we investigated the effect of PELP1 on metabolic pathways  
236 using the Seahorse Cell Energy Phenotype test to measure oxygen consumption rate (OCR) and

237 extracellular acidification rate (ECAR). At baseline, MCF-7 cells expressing cyto PELP1 exhibited  
238 a significant increase in OCR levels compared to LXS and WT PELP1. Under stressed  
239 conditions (i.e. after FCCP and oligomycin), OCR was increased in cyto PELP1 expressing cells  
240 compared to LXS ( $p = 0.0096$ ). ECAR was significantly different in cyto PELP1 expressing cells  
241 compared to LXS at baseline, but WT and cyto PELP1 displayed an increase in ECAR compared  
242 to LXS controls ( $p = 0.046$  and  $0.0045$ ) under stressed conditions (**Figure 2B**). To systematically  
243 test effects on key parameters of mitochondrial function, we performed the Seahorse Mito Stress  
244 test. Cyto PELP1 expression significantly increased basal respiration, compared to LXS and WT  
245 PELP1 ( $p < 0.0001$  and  $0.0001$ ). Furthermore, cyto PELP1 increased ATP-linked respiration,  
246 proton leak, maximal respiration, and non-mitochondrial respiration (**Figure 2C**). Cyto PELP1  
247 expressing cells had a 4-fold increase in glucose uptake compared to WT PELP1 and LXS, as  
248 measured by 2-NBDG (**Figure 2D, Supplementary Figure 6**). Collectively, these results indicate  
249 cyto PELP1 drives HIF-activated metabolic programs (i.e. *PFKFB3*, *PFKFB4*) in 3D culture, and  
250 affects mitochondrial respiration and glycolysis, indicative of metabolic plasticity.

251

### 252 **Inhibition of PFKFBs disrupts PELP1/SRC-3 complexes and tumorsphere formation**

253 We hypothesized that HIF-activated targets PFKFB3 and PFKFB4 are required components of  
254 the PELP1/SRC-3 complex. Co-immunoprecipitation of PFKFB3 or PFKFB4 demonstrated  
255 increased association with PELP1 in cells expressing cyto PELP1 relative to LXS or WT PELP1  
256 (**Figure 3A, 3B**). Treatment with PFK158 and 5MPN, inhibitors of PFKFB3 and PFKFB4  
257 respectively, reduced the PELP1/SRC-3 interaction (**Figure 3C, 3D**). These inhibitors also  
258 blocked PELP1/PFKFB3 and PELP1/PFKFB4 (**Supplementary Figure 7A, 7B**) interactions in  
259 cyto PELP1 expressing cells; similar results were observed with another PFKFB3 inhibitor  
260 (PFK15; **Supplementary Figure 7C, 7D**).

261

262 Next, we tested the effect of PFKFB inhibition on cyto PELP1-induced tumorspheres, an *in vitro*  
263 assay to assess breast CSC activity (11). PFKFB4 knockdown (**Supplementary Figure 8**)  
264 decreased tumorsphere formation in cyto PELP1 expressing cells by ~50%, but not in LXS or  
265 WT PELP1 (**Figure 3E**,  $p = 0.0103$ ). Attempts to stably knockdown PFKFB3 were not successful,  
266 suggesting that PFKFB3 is crucial for cell viability (22). Inhibitors of PFKFB3 and PFKFB4  
267 reduced cyto PELP1-induced tumorspheres, but had no effect on cells expressing either LXS  
268 or WT PELP1. (**Figure 3F, 3G; Supplementary Figure 7E**). To evaluate PFKFB inhibitors in an  
269 alternative PELP1/SRC-3 model, we used a murine tumor cell line (J110) established from the  
270 MMTV-SRC-3 mouse (23). Similar to MCF-7 PELP1 models, PFK158 or 5MPN inhibited

271 tumorsphere formation by ~40% in J110 cells (**Figure 3H**). Western blotting indicated that  
272 PFKFB3 and PFKFB4 protein levels remained unchanged in response to E2, while ER levels  
273 decreased, presumably due to ligand-induced turnover (**Figure 3H**, right). These results indicate  
274 that blocking PFKFB3 or PFKFB4 through knockdown or pharmacological inhibition disrupts  
275 expansion and self-renewal of PELP1-driven CSC populations.

276

### 277 **PFKFB4 reduces *in vivo* expansion of CTCs in cyto PELP1 MIND xenografts**

278 To evaluate if PELP1 promotes tumor formation *in vivo*, we injected MCF-7 WT and cyto PELP1  
279 expressing cells ( $5 \times 10^4$ ) into the inguinal mammary glands of adult female mice (6-8 week old,  
280 4 mice/group) to generate mammary intraductal (MIND) tumors. Both cell lines had 100%  
281 engraftment rates (**Figure 4A, Supplementary Figure 9**). Tumor area (%) calculated from H&E  
282 images of each mammary gland revealed increased tumor volume in cyto PELP1 ( $25.7\% \pm 16.5$ )  
283 compared to WT PELP1 MIND xenografts ( $10.9\% \pm 9.5$ ,  $p = 0.046$ ) (**Figure 4B**).

284

285 Based on our *in vitro* data showing that inhibition of PFKFB4 (knockdown and 5MPN) decreased  
286 tumorspheres, we queried PFKFB4 mRNA levels on OS in METABRIC datasets. High PFKFB4  
287 mRNA expression is associated with decreased OS in all subtypes and ER+ only patient cohorts  
288 (**Supplementary Figure 10**). Therefore, we tested whether PFKFB4 knockdown would impact  
289 MIND tumor growth or the presence of circulating tumor cells (CTCs); a marker of metastatic  
290 potential and associated CSC behavior (24). 5 mice/group were injected with MCF-7 WT or cyto  
291 PELP1 expressing cells harboring either shGFP control or shPFKFB4. 8 weeks post-injection,  
292 mammary glands were fixed and processed for H&E staining (**Supplementary Figure 11**). As in  
293 **Figure 4B**, the difference in means between WT PELP1 shGFP ( $26.8\% \pm 10.2$ ) and cyto PELP1  
294 shGFP ( $41.2\% \pm 17.2$ ) tumor area remained significant ( $p = 0.036$ , **Figure 4C**). However,  
295 knockdown of PFKFB4 in MCF-7 cells expressing either WT PELP1 or cyto PELP1 failed to  
296 significantly affect primary tumor growth. To assess disseminated tumor cells, blood samples  
297 were collected during euthanization and seeded into soft agar assays to detect CTCs. Mice  
298 injected with WT PELP1 (shGFP or shPFKFB4) expressing cells did not exhibit CTC colony  
299 formation. In sharp contrast, blood samples from mice engrafted with cyto PELP1 cells developed  
300 large viable colonies, indicating the presence of CTCs. Knockdown of shPFKFB4 in MCF-7 cyto  
301 PELP1 expressing cells reduced both colony formation ( $p < 0.0492$ ) and colony size ( $p < 0.0016$ )  
302 (**Figure 4D-4F**). These data demonstrate a requirement for PFKFB4 in cyto PELP1-driven CTC  
303 formation and expansion *in vivo*.

304

305 **Targeting PELP1/SRC-3 complexes in therapy resistant breast cancer and PDxO models**  
306 Paclitaxel (Taxol) is a chemotherapy used to treat late stage breast cancer. Increased PELP1,  
307 HIF1 $\alpha$ , and HIF-2 $\alpha$  expression has been observed in triple negative breast cancer (TNBC) cells  
308 in response to Taxol (14). To evaluate whether PELP1 expression affects response to Taxol in  
309 ER+ breast cancer, we treated MCF-7 PELP1 cells (LXSN, WT PELP1, cyto PELP1) cultured as  
310 tumorspheres with Taxol (0 to 125 nM). We assessed tumorsphere formation and calculated IC50  
311 values for each cell line (**Figure 5A**). IC50 (Taxol) for cyto PELP1 expressing cells was ~2-fold  
312 higher than LXSN or WT PELP1. These results suggest that cyto PELP1 expression confers  
313 enhanced Taxol resistance compared to LXSN or WT PELP1.

314  
315 Next, we determined if PELP1/SRC-3 signaling mediates therapy resistance in tamoxifen  
316 resistant (TamR) and paclitaxel-resistant (TaxR) cell lines. HIF and cyto PELP1 regulated genes,  
317 *EPAS1*, *PFKFB3*, and *PFKFB4*, mRNA levels were increased in MCF-7 TaxR (**Figure 5B, top**)  
318 and TamR cells (**Figure 5B, bottom**) relative to MCF-7 parental controls, particularly in 3D  
319 conditions. 3D PELP1 target genes, *NDRG1* and *SOX9* were also upregulated in TaxR and TamR  
320 cells relative to parental MCF-7 cells (**Supplementary Figure 12**). To determine if similar  
321 changes in cellular metabolism occur in MCF-7 TaxR models, we performed Seahorse metabolic  
322 assays. The Cell Energy Phenotype test showed TaxR cells exhibit increased OCR and ECAR at  
323 baseline and stressed conditions relative to controls (**Figure 5C**), indicating increased  
324 mitochondrial respiration and glycolysis. To look at individual effects on OCR, we performed the  
325 Mito Stress test in MCF-7 TaxR models. Similar to cyto PELP1 expressing cells, TaxR cells  
326 showed significant increases in basal and maximal respiration compared to controls (**Figure 5D**).  
327 TaxR cells increased proton leak, spare respiratory capacity, and non-mitochondrial respiration,  
328 but not ATP production as observed in MCF-7 cyto PELP1 expressing cells. TaxR cells also  
329 displayed ~2-fold increase ( $p = 0.0006$ ) in glucose uptake compared to controls (**Figure 5E**).  
330 Together, these data reveal that TamR and TaxR models phenocopy HIF-associated target gene  
331 expression and metabolic plasticity of MCF-7 cyto PELP1 expressing cells, and suggest PELP1  
332 may be a key mediator in therapy resistance.

333  
334 The PELP1/SRC-3 interaction was similarly increased in MCF-7 TaxR (**Figure 5F, top**) and TamR  
335 cells (**Figure 5F, bottom**). Additionally, CD44 $^{hi}$ /CD24 $^{lo}$  ratios were increased in MCF-7 TaxR cells  
336 compared to parental controls (**Supplementary Figure 13**). To test the pharmacological effect of  
337 PFKFB3, PFKFB4, and SRC-3 inhibition, MCF-7 TaxR and TamR cells were seeded as  
338 tumorspheres and treated with PFK158, 5MPN, and SI-2. Both resistant models exhibited

339 increased basal tumorsphere formation when compared to parental controls. 5MPN and SI-2  
340 effectively decreased secondary tumorsphere formation by 71% and 75% in TaxR (**Figure 5G**),  
341 and 88% and 92% in TamR models (**Figure 5H**) compared to vehicle controls. PFK158 (PFKFB3  
342 inhibitor) modestly decreased TaxR and TamR tumorspheres by 17% and 27%. These findings  
343 highlight the overlap of key players involved in PELP1-driven CSC biology and suggest that  
344 PFKFB4 and SRC-3 play a more significant role than PFKFB3 within resistant cell models.

345

346 We hypothesized that tam in combination with PELP1/SRC-3 complex inhibitors (i.e. SI-2 or  
347 5MPN) would be more effective than either inhibitor alone. Combination treatments were  
348 evaluated in several cell lines. In MCF-7 PELP1 models, we tested tam/SI-2, tam/5MPN, and SI-  
349 2/5MPN combinations (**Figure 6A-6C**). Tam/SI-2 and tam/5MPN reduced tumorsphere formation  
350 in cyto PELP1 expressing cells by ~85% ( $p < 0.0001$ ) and 80% ( $p < 0.0001$ ) compared to vehicle.  
351 Single agent treatment with tam or SI-2 also reduced tumorspheres, but to a lesser degree than  
352 combinations. PFK158 co-treatment with tam was not more effective than tam alone and was not  
353 further pursued (**Supplementary Figure 14A**). Effective combinations were then tested in J110  
354 cells (**Supplementary Figure 14B-14D**). Tam, SI-2, and 5MPN alone inhibited tumorspheres by  
355 39, 41, and 28%, while co-treatment did not have dramatic effects. The SI-2/5MPN combination  
356 was most effective in J110 cells, and decreased tumorsphere formation by 60%, most likely  
357 because J110 cells are an SRC-3-derived transgenic mouse mammary tumor cell line (25).

358

359 Because PELP1 confers tamoxifen and Taxol resistance (**Figure 5A**), we also tested the effect  
360 of these agents in resistant cell models. Similar to observations in MCF-7 PELP1 models, tam co-  
361 treatments were more effective when combined with SI-2 or 5MPN in MCF-7 TaxR models  
362 (**Figure 6D, 6E**). The SI-2/5MPN combination was not more effective than individual agents in  
363 TaxR models (**Figure 6F**), suggesting that SRC-3 and PFKFB4 cooperation occurs in tam-  
364 sensitive models. Accordingly, SI-2/5MPN co-treatment in MCF-7 and T47D TamR models  
365 reduced tumorsphere formation by 77% ( $p < 0.0001$ ) and 75% ( $p < 0.0001$ ) (**Supplementary**  
366 **Figure 14E, 14F**).

367

368 To further explore the therapeutic potential of inhibitor combinations, we utilized pre-clinical  
369 patient-derived organoid models (PDxO; ). Synergy screens were used to test combinations  
370 identified from **Figure 6** on proliferation using CellTiter Glo assays in PDxO models (HCl-003, -  
371 011, and -017). Zero Interaction Potency (ZIP) scores are shown in contour maps for tam/SI-2,  
372 tam/5MPN, and SI-2/5MPN treatments (**Figure 7A-7C, Supplementary Figure 15A-15C**), and

373 indicate the percent a response is higher ( $>1$ ) or lower ( $<1$ ) than the expected response for the  
374 dose combination ( $\delta$ -score). While the  $\delta$ -score across the range of dose combinations tested were  
375 relatively weak, significant peaks of synergism ( $\delta$ -score  $>5$ ) were observed. The most synergistic  
376 area scores are summarized in **Figure 7D**. The tam/SI-2  $\delta$ -scores (~1 to 3) were the lowest and  
377 contour maps indicate antagonism. The SI-2/5MPN  $\delta$ -scores (~5 to 13.5) are lower than the  
378 tam/5MPN scores (~12 to 27) suggesting the tam/5MPN combination is more effective at inhibiting  
379 PDxO proliferation. Next, we evaluated two of the ER+ PDxO models (HCl-003, HCl-017) for  
380 expression of PELP1, SRC-3, PFKFB3, PFKFB4, and ER mRNA and protein (**Supplementary**  
381 **Figure 15D, Figure 7E**). MCF-7 and T47D cell lines were included as controls. Both HCl-003 and  
382 HCl-017 express all proteins tested. Interestingly, PDxO models have higher levels of PFKFB  
383 proteins compared to MCF-7 and T47D cells. Next, we tested inhibitor combinations on CSC  
384 activity in PDxO models. PDxOs were grown to maturity, pre-treated for 3 days, then dissociated  
385 and seeded into tumorspheres in the presence of inhibitors. Individual treatments (tam, SI-2,  
386 5MPN) reduced tumorsphere formation in both PDxO models by 36 to 62% (**Figure 7F-7H**). The  
387 tam/SI-2 combination was not more effective than individual treatment (**Figure 7F**). In contrast,  
388 tam/5MPN was more effective than tam or 5MPN alone and reduced tumorspheres by ~71% and  
389 ~90% in HCl-003 and HCl-017 (**Figure 7G**). SI-2/5MPN co-treatment was more effective than SI-  
390 2 or 5MPN alone and reduced tumorsphere formation by ~71% ( $p < 0.0001$ ) and ~74% ( $p <$   
391 0.0001) in HCl-003 and HCl-017 (**Figure 7H**). These results demonstrate that blocking the  
392 PELP1/SRC-3 complex and associated binding partners is an effective approach to targeting CSC  
393 populations in multiple models of advanced breast cancer. Taken together, these studies provide  
394 promising alternative approaches to target non-ER mediators and overcome emergence of  
395 chemotherapy and endocrine resistance.

396

397

## 398 **DISCUSSION**

399 The CSC hypothesis postulates that tumors contain a subset population (i.e. CSCs) that share  
400 properties of normal stem cells including self-renewal, differentiation, and capacity to repopulate  
401 the heterogeneous tumor (9). CSCs are proposed to have heightened resistance to cancer  
402 therapies due to their relative quiescent state (26), enabling this population to evade standard of  
403 care treatments that target proliferating bulk tumor cells. Herein, we sought to define mechanisms  
404 of SR co-activator driven CSC survival and expansion in ER+ breast cancer. We conclude that  
405 SR co-activator complexes enhance CSC activity and therapy resistance by promoting metabolic  
406 plasticity. Inhibiting these complexes and/or associated binding partners in combination with

407 endocrine therapies may be an effective strategy to block CSC survival and self-renewal, and  
408 breast cancer progression.

409  
410 Our findings further implicate PELP1/SRC-3 complexes as mediators of CSC activity. We  
411 observed similarities in gene expression, cell metabolism, and sensitivity to inhibitors of PELP1  
412 binding partners in endocrine and chemotherapy resistant ER+ cell lines. Although PELP1  
413 expression contributes to cell survival in response to Taxol in TNBC (14), our studies are the first  
414 to demonstrate enhanced Taxol tolerance in the context of cyto PELP1 in ER+ breast cancer. Our  
415 results in TaxR models highlight the impact of targeting PELP1 binding partners involved in  
416 PELP1-mediated CSC self-renewal (**Figure 5**). Mesenchymal stem cells (27) and ovarian cancer  
417 cells (28) achieve Taxol resistance by shifting to G0 and entering quiescence. PELP1 is a  
418 substrate of CDKs and modulates G1/S cell cycle progression (29). PELP1 may confer Taxol  
419 resistance in part through cell cycle regulation, albeit further studies are needed to define  
420 cytoplasmic PELP1-specific contributions in this context.

421  
422 Contributing factors to CSC survival include metabolic plasticity, which enables adaptation to  
423 diverse tumor environments. For example, inhibition of glycolysis reduces breast and lung CSCs  
424 (30). Glycolytic reprogramming has been documented in breast cancer cells during EMT, resulting  
425 in acquisition of CSC-like characteristics and tumorigenicity (31). In contrast, breast CSCs utilize  
426 oxidative phosphorylation (OXPHOS) as their primary metabolic program (32). Bulk tumor cells  
427 depend chiefly on glycolysis, whereas tumors enriched for breast CSCs rely mainly on OXPHOS  
428 (33). RNA-seq analysis indicated cytoplasmic PELP1 imparts increased HIF-activated pathways  
429 under normoxic 3D conditions to enrich for CSCs. ChIP assays demonstrated *EPAS1* (i.e. HIF-  
430 2 $\alpha$ ) recruitment to HRE regions of the PELP1 promoter in TNBC cells (34). Thus, PELP1-induced  
431 HIF pathways may serve as a feed-forward mechanism to drive metabolic genes programs.  
432 PFKFB3 and PFKFB4 are required for glycolytic response to hypoxia via HIF-1 $\alpha$  activation (20).  
433 We demonstrated that cyto PELP1 expressing cells increased glycolysis and mitochondrial  
434 respiration. Additional studies are needed to define the bioenergetics driving this plasticity.  
435 PFKFB4-mediated SRC-3 Ser857 phosphorylation has essential functions in lung and breast  
436 cancer metastasis and metabolism (35). Phosphorylation of SRC-3 Ser857 promotes SRC-3  
437 association with transcription factor *ATF4* to mediate non-oxidative pentose phosphate pathway  
438 and purine synthesis. This study (35) did not evaluate SRC-3 in the context of CSCs, although  
439 SRC-3 has been linked to CSC activity (10,11). Our IPA studies also identified *ATF4* pathway

440 activation (**Figure 1**); upregulation of *ATF4* could explain the correlation between PFKFB4 and  
441 PELP1/SRC-3-driven CSCs.

442

443 PFKFB inhibitors are emerging as promising treatments in endocrine and chemotherapy-resistant  
444 ER+ breast cancer (36). PFKFB3 inhibitor, PFK158, displays broad anti-tumor and  
445 immunomodulatory effects in human and preclinical mouse models (37) and was evaluated in a  
446 Phase I clinical trial with no significant adverse effects (38). The prognostic value of PFKFB4  
447 expression was evaluated in 200 tumor samples from stage I to III breast cancer patients. Similar  
448 to our METABRIC analysis (**Supplementary Figure 10**), elevated PFKFB4 expression was  
449 associated with poor disease-free survival and overall survival in ER+, HER2+, or TNBC patients  
450 (39). PFKFB4 inhibitors (e.g. 5MPN) have not yet moved to clinical trials. Studies have suggested  
451 correlative and mechanistic links between PFKFBs and CSCs. *PFKFB3* was upregulated in a  
452 CD44<sup>hi</sup>CD24<sup>lo</sup> gene signature correlated to risk of distant metastasis and poor outcome in breast  
453 cancer patients (40). A cleaved product of CD44 (CD44ICD) promoted breast cancer stemness  
454 via PFKFB4-mediated glycolysis (41). Notably, 5MPN treatment suppressed CD44ICD-induced  
455 tumorigenesis. We have further implicated PFKFBs as drivers of CSC activity by demonstrating  
456 5MPN reduces tumorspheres as a single agent or in combination treatments in multiple ER+  
457 breast cancer models, including treatment resistant cells (TaxR, TamR), murine tumor cells, and  
458 pre-clinical PDxOs. Our data shows that treatment with 5MPN in combination with SI-2 or tam  
459 inhibits PDxO proliferation (**Figure 7**), but importantly also targets the CSC population. Studies in  
460 breast cancer patients indicate that EMT and CSC markers are present in CTC populations, which  
461 have high metastatic potential (42). Our MIND xenografts demonstrate PFKFB4 knockdown does  
462 not have an effect on primary tumor burden, but reduces CTC populations (**Figure 4**). These data  
463 suggest PFKFB4 inhibition is an effective strategy for targeting CSCs and CTCs in ER+ breast  
464 cancer. Future work should involve assessing overlap between PFKFB4-modulated CSC and  
465 CTC populations by evaluating the impact of 5MPN inhibitor combinations *in vivo*.

466

467 To evaluate the impact of SR co-activators on CSCs, it will be important that future studies  
468 consider SR-driven contributions. Breast CSCs are reported to be mostly ER negative (43), which  
469 may explain their poor response to anti-estrogens. However, SR+ cells contribute to CSC biology  
470 through SR-dependent (namely PR) paracrine factors (44). For example, breast CSC self-renewal  
471 was stimulated after anti-estrogen treatment of breast cancer cells or PDX models (45,46). These  
472 studies suggest anti-estrogen therapies may initially slow tumor growth, but concurrently evoke  
473 plasticity and CSC activity in non-proliferative tumor cells. Notably, PELP1-containing complexes

474 include ER and PR (47). PRs but not ER are potent drivers of stem and progenitor cell expansion  
475 in normal and neoplastic breast tissues (48). We have recently defined a requirement for  
476 phosphorylated and inducible PR in CSC biology (49), insulin hypersensitivity, and tam resistance  
477 in ER+ breast cancer (13). CSC outgrowth in therapy resistant ER+/PR-low breast cancer models  
478 is blocked by PR knockdown or antiprogestins (13). These findings suggest PELP1/SRC-3  
479 complexes enable constitutive SR activity in sub-populations that easily bypass endocrine  
480 therapies. Antagonizing estrogen signaling may select for cells that display ligand-independent  
481 ER and PR, resulting in increased proportions of breast CSCs, and subsequently promote  
482 metastasis. Therefore, treatment should include endocrine therapy in combination with targeted  
483 therapies that block mediators of CSC survival and self-renewal as defined herein (i.e. PFKFBs).

484

485

## 486 CONCLUSION

487 Our work demonstrates that targeting SR co-activators and associated binding partners involved  
488 in driving CSC survival, self-renewal, and metabolic plasticity may impede breast cancer  
489 progression and has the potential to lead to improved outcomes. Identifying the mechanisms that  
490 mediate recurrent ER+ tumor cell populations (e.g. CSCs, CTCs) will enable specific targeting  
491 within heterogeneous breast tumors to overcome endocrine and chemotherapy resistance.

492

493

## 494 ACKNOWLEDGEMENTS

495 We thank Bruce Lindgren for biostatistics support, and the Masonic Cancer Center Biostatistics  
496 and Bioinformatics, Analytical Biochemistry, and Flow Cytometry shared resources. We also  
497 thank Zohar Sachs and Michael Franklin for critical reading of this manuscript.

498

499

500

501

502

503

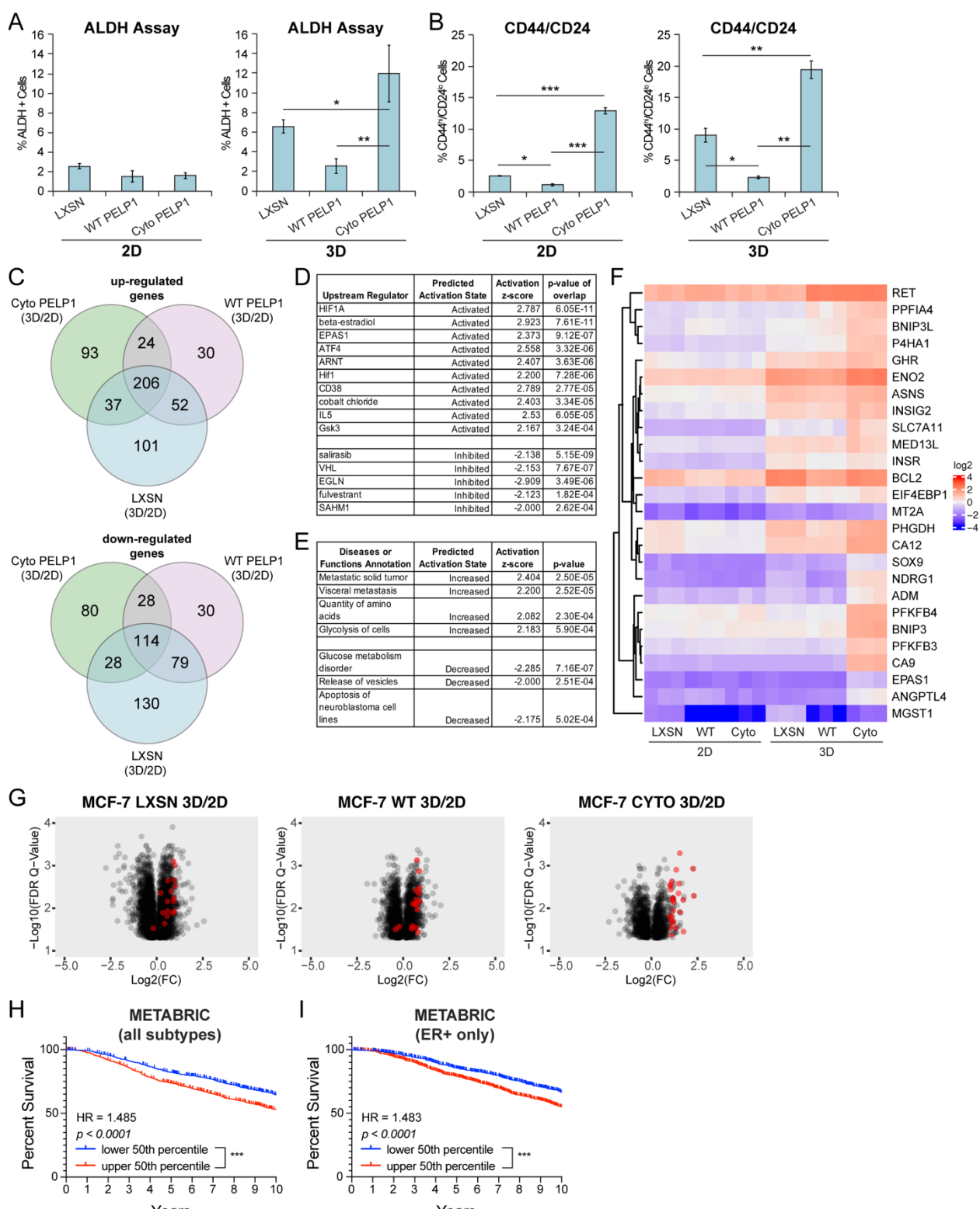
504

505

506

507

508 **FIGURE LEGENDS**



509

510 **Figure 1.** PELP1-induced gene expression is altered in 3D conditions. **(A)** ALDH activity and **(B)**  
511 CD44<sup>hi</sup>/CD24<sup>lo</sup> populations in MCF-7 PELP1 cells. **(C)** Venn diagrams showing unique genes up

512 or downregulated >2-fold in MCF-7 PELP1 cells (3D vs. 2D). IPA analysis of (**D**) upstream  
513 regulators and (**E**) diseases or functions. (**F**) Representative heat-map showing log2(FPKM)  
514 values of cyto PELP1 gene signature. (**G**) Volcano plots of 3D vs. 2D comparison of MCF-7  
515 PELP1 cells. X-axis is Log2(fold change) and Y-axis represent -Log 10 Benjamini-Hochberg  
516 corrected Q-values. Kaplan-Meier curves for upper and lower 50<sup>th</sup> percentile of cyto PELP1 gene  
517 signature expression in the METABRIC (**H**) all subtypes and (**I**) ER+ only patient cohorts. Graphed  
518 data represent the mean ± SD (n = 3). \* p < 0.05, \*\* p < 0.01, \*\*\* p < 0.001.

519

520

521

522

523

524

525

526

527

528

529

530

531

532

533

534

535

536

537

538

539

540

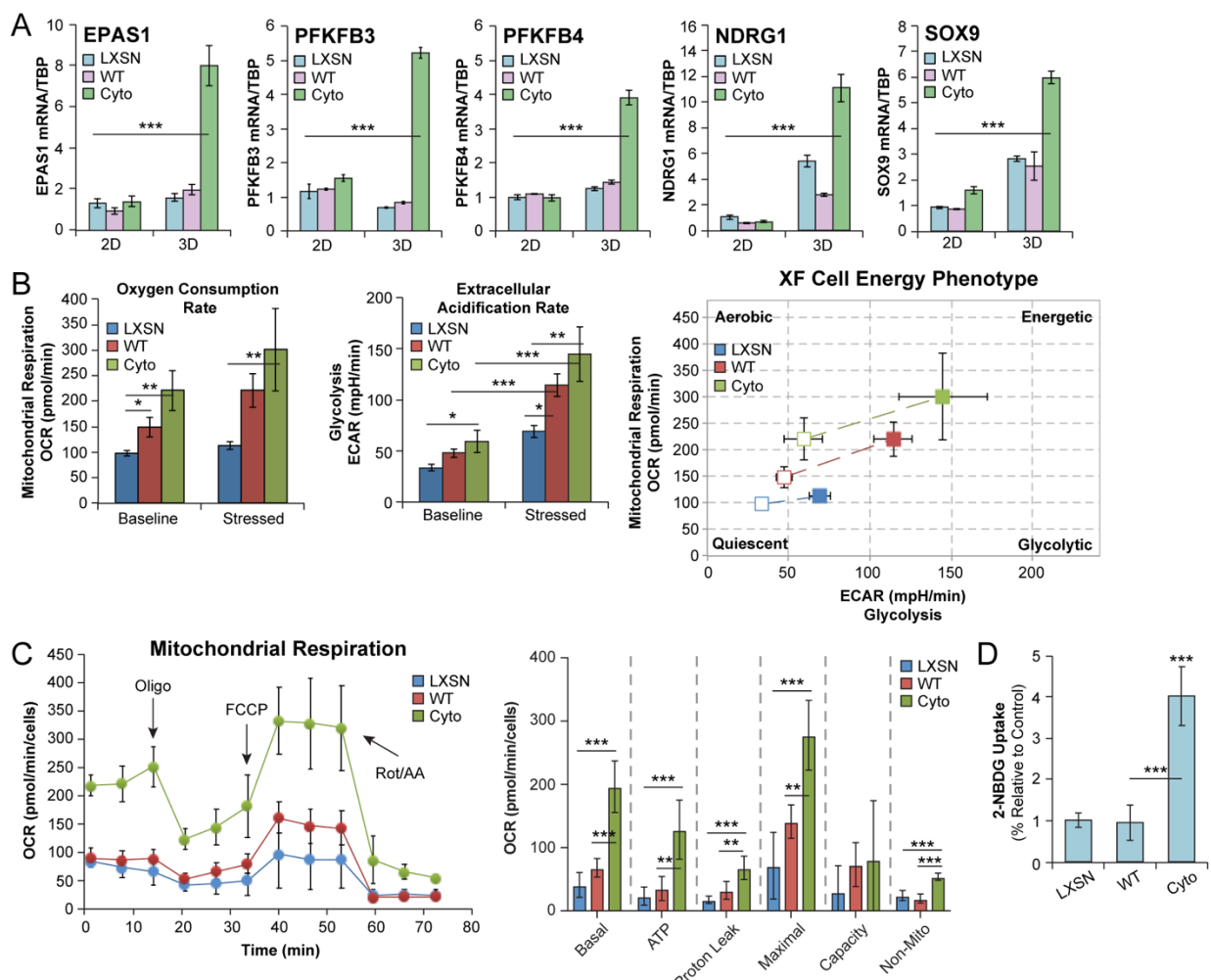
541

542

543

544

545



546

547 **Figure 2. PELP1 cytoplasmic signaling upregulates HIF-activated metabolic pathways. (A)** mRNA  
 548 levels of *EPAS1*, *PFKFB3*, *PFKFB4*, *NDRG1*, and *SOX9* in MCF-7 PELP1 cells. **(B)** OCR and  
 549 ECAR measured in MCF-7 PELP1 cells by Seahorse Cell Energy Phenotype test. **(C)** OCR  
 550 measured in MCF-7 PELP1 cells by Seahorse Mito Stress test. **(D)** Glucose uptake in cells treated  
 551 with 2-NBDG (10  $\mu$ M). 2-NBDG uptake is represented as % cells relative to control. Graphed data  
 552 represent the mean  $\pm$  SD ( $n = 3$ ). \*  $p < 0.05$ , \*\*  $p < 0.01$ , \*\*\*  $p < 0.001$ .

553

554

555

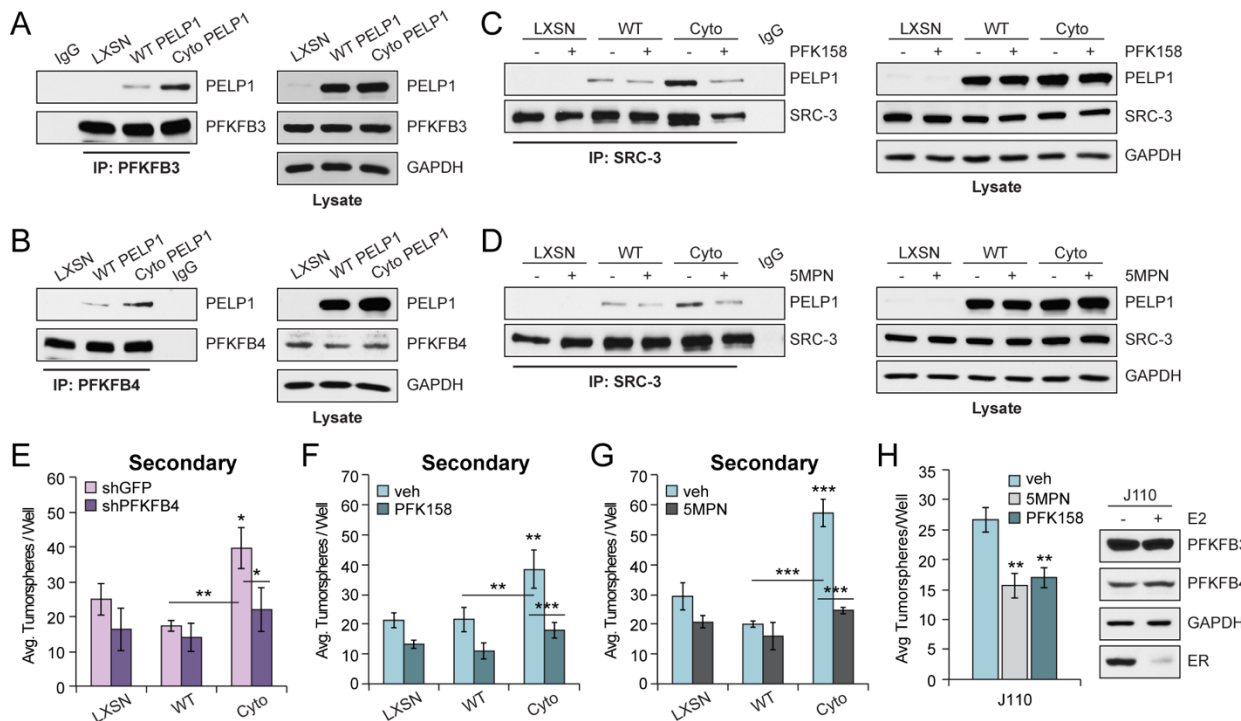
556

557

558

559

560



561

562 **Figure 3. PFKFB inhibition blocks PELP1/SRC-3 signaling. Co-immunoprecipitation of (A) PELP1**

563 and PFKFB3 or (B) PFKFB4 in MCF-7 PELP1 cells. Co-immunoprecipitation of PELP1 and SRC-

564 3 in MCF-7 PELP1 cells treated with vehicle (DMSO), (C) PFK158 (100 nM), or (D) 5MPN (5  $\mu$ M).

565 Cell lysate controls (right). (E) Secondary tumorsphere assays in MCF-7 PELP1 shGFP control

566 or shPFKFB4 knockdown cells. Secondary tumorsphere assays in MCF-7 PELP1 cells treated

567 with vehicle, (F) PFK158 or (G) 5MPN. (H) Secondary tumorsphere assays in J110 cells treated

568 with vehicle, PFK158, or 5MPN. Western blot shows PFKFB3 and PFKFB4 protein in J110 cells.

569 Graphed data represent the mean  $\pm$  SD (n = 3). \* p < 0.05, \*\* p < 0.01, \*\*\* p < 0.001.

570

571

572

573

574

575

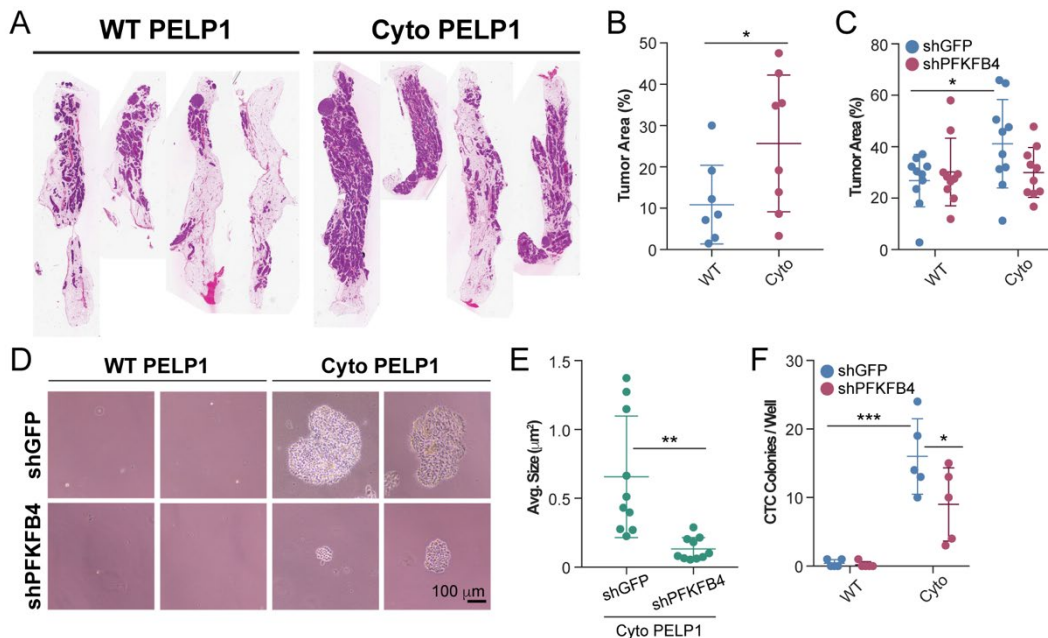
576

577

578

579

580



581

582 **Figure 4.** PFKFB4 knockdown abrogates cyto PELP1 CTCs in MIND xenograft models. **(A)**  
583 Representative H&E stains from MIND glands (WT and cyto PELP1). **(B)** Tumor area (%)  
584 calculated from H&E sections from **(A)**. **(C)** Tumor area (%) calculated from H&E sections from  
585 WT and cyto PELP1 (shGFP, shPFKFB4) MIND glands. **(D)** Representative images of CTCs from  
586 blood samples collected from mice injected with WT or cyto PELP1 (shGFP, shPFKFB4) cells.  
587 **(E)** Average size of soft agar colonies (CTCs) from **(D)**. **(F)** Average number of colonies/well  
588 (CTCs). Graphed data represent the mean  $\pm$  SD (n = 5). \* p < 0.05, \*\* p < 0.01, \*\*\* p < 0.001.

589

590

591

592

593

594

595

596

597

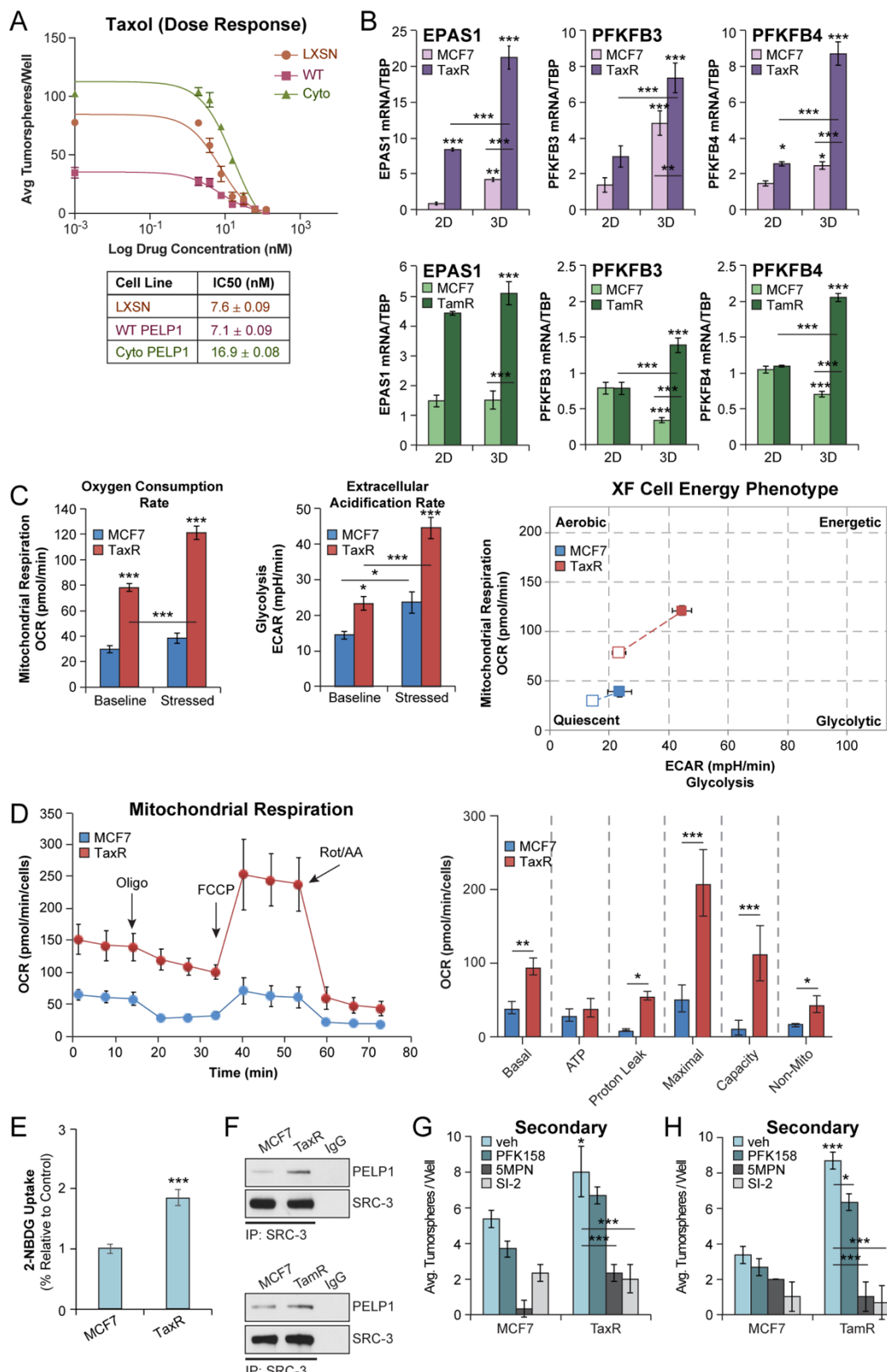
598

599

600

601

602



603

604 **Figure 5.** Therapy resistant models phenocopy cyto PELP1 cancer biology. **(A)** Taxol dose  
605 response in MCF-7 PELP1 cells (0-125 nM Taxol). **(B)** mRNA levels of *EPAS1*, *PFKFB3*, and

606 *PFKFB4* in MCF-7 TaxR (*top*) or TamR (*bottom*) cells cultured in 2D or 3D conditions. (**C**) OCR  
607 and ECAR measured in MCF-7 TaxR cells by Seahorse Cell Energy Phenotype test. (**D**) OCR  
608 measured in MCF-7 TaxR cells by Seahorse Mito Stress test. (**E**) Glucose uptake in cells treated  
609 with 2-NBDG (10  $\mu$ M). (**F**) Co-immunoprecipitation of PELP1 and SRC-3 in MCF-7 TaxR (*top*) or  
610 TamR (*bottom*) cells. Secondary tumorsphere assays in (**G**) MCF-7 TaxR and (**H**) MCF-7 TamR  
611 cells treated with vehicle (DMSO), PFK158 (100 nM), 5MPN (5  $\mu$ M), or SI-2 (100 nM). Graphed  
612 data represent the mean  $\pm$  SD (n = 3). \* p < 0.05, \*\* p < 0.01, \*\*\* p < 0.001.

613

614

615

616

617

618

619

620

621

622

623

624

625

626

627

628

629

630

631

632

633

634

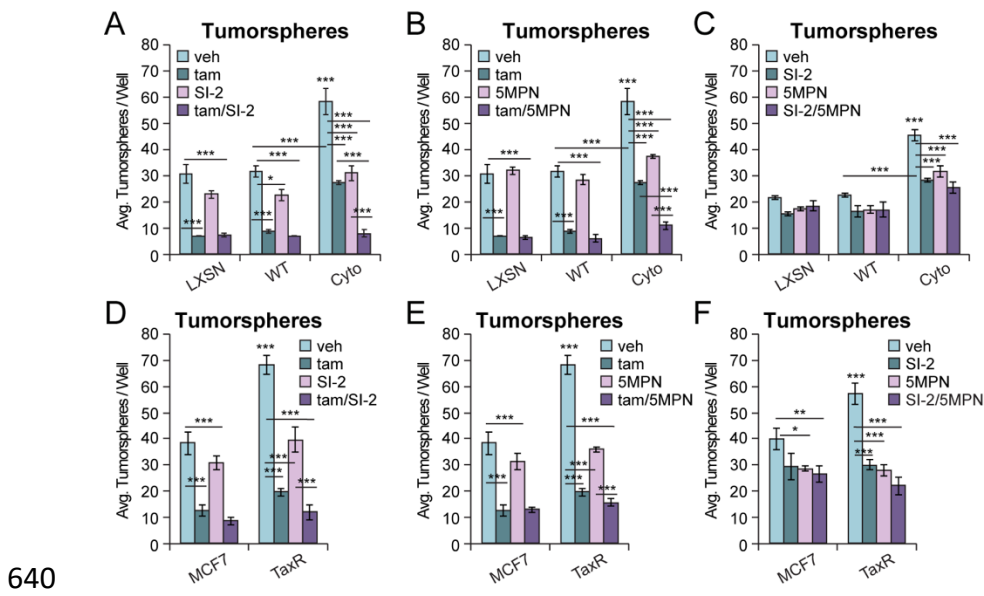
635

636

637

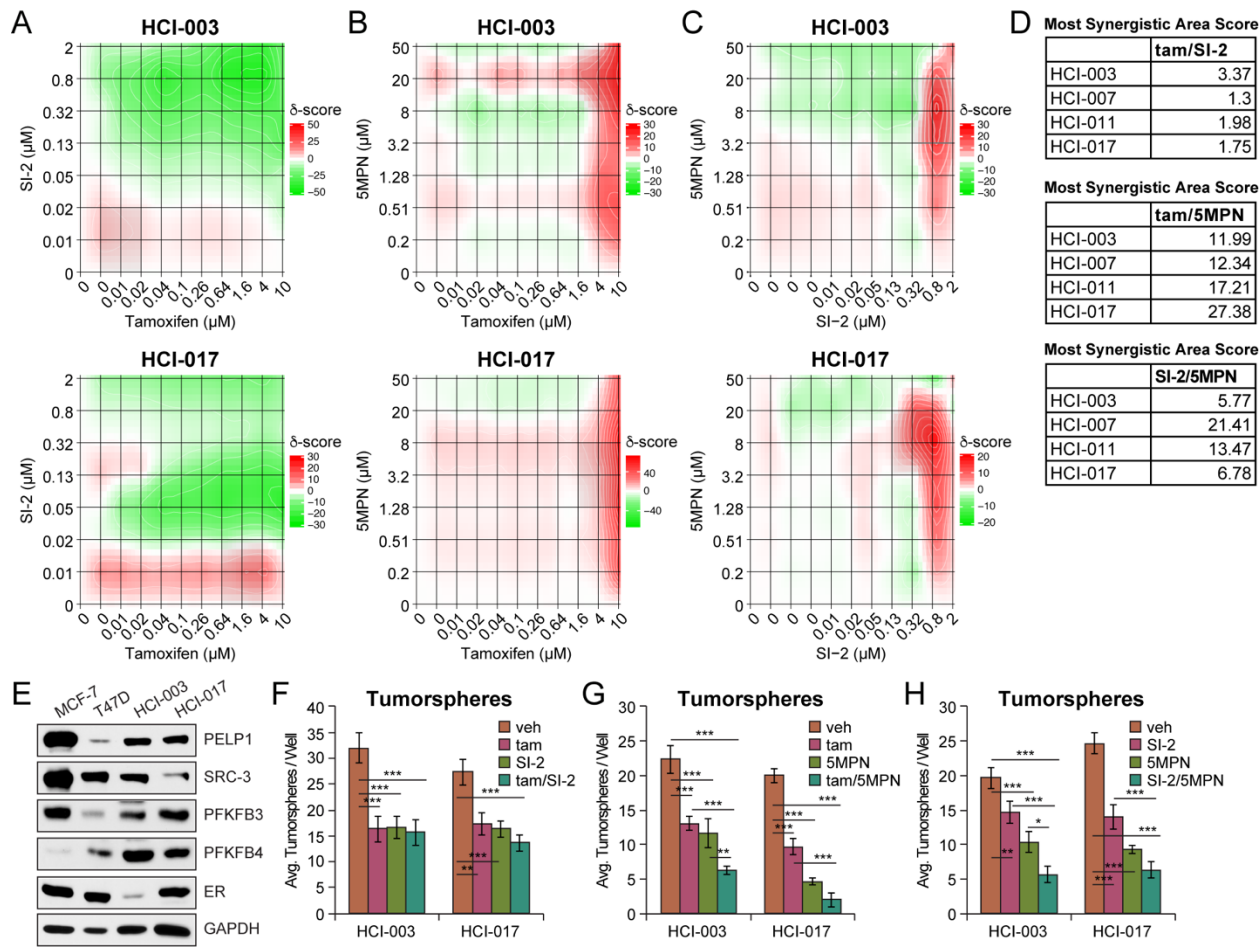
638

639



640  
641 **Figure 6.** Endocrine therapies exhibit combinatorial effects with PELP1 complex inhibitors.  
642 Tumorsphere assays in MCF-7 PELP1 cells treated with: (A) tam/SI-2, (B) tam/5MPN, or (C) SI-  
643 2/5MPN. Tumorsphere assays in MCF-7 TaxR cells treated with: (D) tam/SI-2, (E) tam/5MPN, or  
644 (F) SI-2/5MPN. Concentrations: tam (100 nM), 5MPN (5  $\mu$ M), SI-2 (100 nM). Graphed data  
645 represent the mean  $\pm$  SD (n = 3). \* p < 0.05, \*\* p < 0.01, \*\*\* p < 0.001.

646  
647  
648  
649  
650  
651  
652  
653  
654  
655  
656  
657  
658  
659  
660  
661  
662



663 **Figure 7.** Co-treatments in preclinical ER+ PDxO models target CSCs. CellTiter Glo assays in  
664 HCl-003 and -017 PDxOs co-treated with (A) tam/SI-2, (B) tam/5MPN, or (C) SI-2/5MPN. (D)  
665 Tables summarizing most synergistic area scores from 7A-C and SFigure 15A-15C. (E) Western  
666 blot of PELP1, SRC-3, PFKFB3, PFKFB4, and ER protein levels in HCl-003 and HCl-017.  
667 Tumorsphere assays in HCl-003 and HCl-017 PDxOs co-treated with (F) tam/SI-2, (G)  
668 tam/5MPN, or (H) SI-2/5MPN. Prior to assay, PDxO models were pre-treated with the indicated  
669 compounds for 3 days and subjected to continued treatment during the assay. Concentrations:  
670 tam (100 nM), 5MPN (5 μM), SI-2 (100 nM). Graphed data represent the mean ± SD (n = 3). \* p  
671 < 0.05, \*\* p < 0.01, \*\*\* p < 0.001.

673

674

675

676

677

678

679 **REFERENCES**

- 680 1. Vadlamudi RK, Wang RA, Mazumdar A, Kim Y, Shin J, Sahin A, et al. Molecular cloning  
681 and characterization of PELP1, a novel human coregulator of estrogen receptor alpha. *J  
682 Biol Chem* 2001;276(41):38272-9.
- 683 2. Xu J, Liao L, Ning G, Yoshida-Komiya H, Deng C, O'Malley BW. The steroid receptor  
684 coactivator SRC-3 (p/CIP/RAC3/AIB1/ACTR/TRAM-1) is required for normal growth,  
685 puberty, female reproductive function, and mammary gland development. *Proc Natl  
686 Acad Sci U S A* 2000;97(12):6379-84.
- 687 3. Habashy HO, Powe DG, Rakha EA, Ball G, Macmillan RD, Green AR, et al. The prognostic  
688 significance of PELP1 expression in invasive breast cancer with emphasis on the ER-  
689 positive luminal-like subtype. *Breast Cancer Res Treat* 2010;120(3):603-12.
- 690 4. Kumar R, Zhang H, Holm C, Vadlamudi RK, Landberg G, Rayala SK. Extranuclear  
691 coactivator signaling confers insensitivity to tamoxifen. *Clin Cancer Res*  
692 2009;15(12):4123-30.
- 693 5. Vadlamudi RK, Manavathi B, Balasenthil S, Nair SS, Yang Z, Sahin AA, et al. Functional  
694 implications of altered subcellular localization of PELP1 in breast cancer cells. *Cancer Res*  
695 2005;65(17):7724-32.
- 696 6. Burandt E, Jens G, Holst F, Janicke F, Muller V, Quaas A, et al. Prognostic relevance of  
697 AIB1 (NCoA3) amplification and overexpression in breast cancer. *Breast Cancer Res  
698 Treat* 2013;137(3):745-53.
- 699 7. Louie MC, Zou JX, Rabinovich A, Chen HW. ACTR/AIB1 functions as an E2F1 coactivator  
700 to promote breast cancer cell proliferation and antiestrogen resistance. *Mol Cell Biol*  
701 2004;24(12):5157-71.
- 702 8. Osborne CK, Bardou V, Hopp TA, Chamness GC, Hilsenbeck SG, Fuqua SA, et al. Role of  
703 the estrogen receptor coactivator AIB1 (SRC-3) and HER-2/neu in tamoxifen resistance  
704 in breast cancer. *J Natl Cancer Inst* 2003;95(5):353-61.
- 705 9. Visvader JE, Lindeman GJ. Cancer stem cells: current status and evolving complexities.  
706 *Cell Stem Cell* 2012;10(6):717-28.
- 707 10. Rohira AD, Yan F, Wang L, Wang J, Zhou S, Lu A, et al. Targeting SRC Coactivators Blocks  
708 the Tumor-Initiating Capacity of Cancer Stem-like Cells. *Cancer Res* 2017;77(16):4293-  
709 304.
- 710 11. Truong TH, Hu H, Temiz NA, Hagen KM, Girard BJ, Brady NJ, et al. Cancer Stem Cell  
711 Phenotypes in ER(+) Breast Cancer Models Are Promoted by PELP1/AIB1 Complexes.  
712 *Mol Cancer Res* 2018;16(4):707-19.
- 713 12. Yang Y, Chan JY, Temiz NA, Yee D. Insulin Receptor Substrate Suppression by the  
714 Tyrphostin NT157 Inhibits Responses to Insulin-Like Growth Factor-I and Insulin in  
715 Breast Cancer Cells. *Horm Cancer* 2018;9(6):371-82.
- 716 13. Dwyer AR, Truong TH, Perez Kerkvliet C, Paul KV, Kabos P, Sartorius CA, et al. Insulin  
717 Receptor Substrate-1 (IRS-1) Mediates Progesterone Receptor-Driven Stemness and  
718 Endocrine Resistance in Estrogen Receptor+ Breast Cancer *Br J Cancer* 2020;Manuscript  
719 Accepted.

720 14. Regan Anderson TM, Ma S, Perez Kerkvliet C, Peng Y, Helle TM, Krutilina RI, et al. Taxol  
721 Induces Brk-dependent Prosurvival Phenotypes in TNBC Cells through an AhR/GR/HIF-  
722 driven Signaling Axis. *Mol Cancer Res* 2018;16(11):1761-72.

723 15. Yadav B, Wennerberg K, Aittokallio T, Tang J. Searching for Drug Synergy in Complex  
724 Dose-Response Landscapes Using an Interaction Potency Model. *Comput Struct  
725 Biotechnol J* 2015;13:504-13.

726 16. Ianevski A, Giri AK, Aittokallio T. SynergyFinder 2.0: visual analytics of multi-drug  
727 combination synergies. *Nucleic Acids Res* 2020;48(W1):W488-W93.

728 17. Behbod F, Kittrell FS, LaMarca H, Edwards D, Kerbawy S, Heestand JC, et al. An  
729 intraductal human-in-mouse transplantation model mimics the subtypes of ductal  
730 carcinoma *in situ*. *Breast Cancer Res* 2009;11(5):R66.

731 18. Sflomos G, Dormoy V, Metsalu T, Jeitziner R, Battista L, Scabia V, et al. A Preclinical  
732 Model for ERalpha-Positive Breast Cancer Points to the Epithelial Microenvironment as  
733 Determinant of Luminal Phenotype and Hormone Response. *Cancer Cell*  
734 2016;29(3):407-22.

735 19. Liu Y, Nenutil R, Appleyard MV, Murray K, Boylan M, Thompson AM, et al. Lack of  
736 correlation of stem cell markers in breast cancer stem cells. *Br J Cancer*  
737 2014;110(8):2063-71.

738 20. Chesney J, Clark J, Klarer AC, Imbert-Fernandez Y, Lane AN, Telang S. Fructose-2,6-  
739 bisphosphate synthesis by 6-phosphofructo-2-kinase/fructose-2,6-bisphosphatase 4  
740 (PFKFB4) is required for the glycolytic response to hypoxia and tumor growth.  
741 *Oncotarget* 2014;5(16):6670-86.

742 21. Kim JW, Dang CV. Cancer's molecular sweet tooth and the Warburg effect. *Cancer Res*  
743 2006;66(18):8927-30.

744 22. Shi L, Pan H, Liu Z, Xie J, Han W. Roles of PFKFB3 in cancer. *Signal Transduct Target Ther*  
745 2017;2:17044.

746 23. Torres-Arzayus MI, Font de Mora J, Yuan J, Vazquez F, Bronson R, Rue M, et al. High  
747 tumor incidence and activation of the PI3K/AKT pathway in transgenic mice define AIB1  
748 as an oncogene. *Cancer Cell* 2004;6(3):263-74.

749 24. Kilgour E, Rothwell DG, Brady G, Dive C. Liquid Biopsy-Based Biomarkers of Treatment  
750 Response and Resistance. *Cancer Cell* 2020;37(4):485-95.

751 25. Torres-Arzayus MI, Yuan J, DellaGatta JL, Lane H, Kung AL, Brown M. Targeting the AIB1  
752 oncogene through mammalian target of rapamycin inhibition in the mammary gland.  
753 *Cancer Res* 2006;66(23):11381-8.

754 26. Moore N, Lyle S. Quiescent, slow-cycling stem cell populations in cancer: a review of the  
755 evidence and discussion of significance. *J Oncol* 2011;2011.

756 27. Bosco DB, Kenworthy R, Zorio DA, Sang QX. Human mesenchymal stem cells are  
757 resistant to Paclitaxel by adopting a non-proliferative fibroblastic state. *PLoS One*  
758 2015;10(6):e0128511.

759 28. Wang X, Pan L, Mao N, Sun L, Qin X, Yin J. Cell-cycle synchronization reverses Taxol  
760 resistance of human ovarian cancer cell lines. *Cancer Cell Int* 2013;13(1):77.

761 29. Nair BC, Nair SS, Chakravarty D, Challa R, Manavathi B, Yew PR, et al. Cyclin-dependent  
762 kinase-mediated phosphorylation plays a critical role in the oncogenic functions of  
763 PELP1. *Cancer Res* 2010;70(18):7166-75.

764 30. O'Neill S, Porter RK, McNamee N, Martinez VG, O'Driscoll L. 2-Deoxy-D-Glucose inhibits  
765 aggressive triple-negative breast cancer cells by targeting glycolysis and the cancer stem  
766 cell phenotype. *Sci Rep* 2019;9(1):3788.

767 31. Dong C, Yuan T, Wu Y, Wang Y, Fan TW, Miriyala S, et al. Loss of FBP1 by Snail-mediated  
768 repression provides metabolic advantages in basal-like breast cancer. *Cancer Cell*  
769 2013;23(3):316-31.

770 32. Vlashi E, Lagadec C, Vergnes L, Reue K, Frohnen P, Chan M, et al. Metabolic differences  
771 in breast cancer stem cells and differentiated progeny. *Breast Cancer Res Treat*  
772 2014;146(3):525-34.

773 33. Banerjee A, Arvinrad P, Darley M, Laversin SA, Parker R, Rose-Zerilli MJ, et al. The  
774 effects of restricted glycolysis on stem-cell like characteristics of breast cancer cells.  
775 *Oncotarget* 2018;9(33):23274-88.

776 34. Regan Anderson TM, Ma SH, Raj GV, Cidlowski JA, Helle TM, Knutson TP, et al. Breast  
777 Tumor Kinase (Brk/PTK6) Is Induced by HIF, Glucocorticoid Receptor, and PELP1-  
778 Mediated Stress Signaling in Triple-Negative Breast Cancer. *Cancer Res* 2016;76(6):1653-  
779 63.

780 35. Dasgupta S, Rajapakshe K, Zhu B, Nikolai BC, Yi P, Putluri N, et al. Metabolic enzyme  
781 PFKFB4 activates transcriptional coactivator SRC-3 to drive breast cancer. *Nature*  
782 2018;556(7700):249-54.

783 36. Mondal S, Roy D, Sarkar Bhattacharya S, Jin L, Jung D, Zhang S, et al. Therapeutic  
784 targeting of PFKFB3 with a novel glycolytic inhibitor PFK158 promotes lipophagy and  
785 chemosensitivity in gynecologic cancers. *Int J Cancer* 2019;144(1):178-89.

786 37. Telang S, Yaddanapudi K, Grewal J, Redman R, Fu S, Pohlmann P, et al. Abstract B90:  
787 PFK-158 is a first-in-human inhibitor of PFKFB3 that selectively suppresses glucose  
788 metabolism of cancer cells and inhibits the immunosuppressive Th17 cells and MDSCs in  
789 advanced cancer patients. *Cancer Res* 2016;76(24 Supplement):B90.

790 38. Redman R, Pohlmann P, Kurman M, Tapolsky GH, Chesney J. Abstract CT206: PFK-158,  
791 first-in-man and first-in-class inhibitor of PFKFB3/ glycolysis: A phase I, dose escalation,  
792 multi-center study in patients with advanced solid malignancies. *Cancer Res* 2015;75(15  
793 Supplement):CT206.

794 39. Yao L, Wang L, Cao ZG, Hu X, Shao ZM. High expression of metabolic enzyme PFKFB4 is  
795 associated with poor prognosis of operable breast cancer. *Cancer Cell Int* 2019;19:165.

796 40. Marotta LL, Almendro V, Marusyk A, Shipitsin M, Schemme J, Walker SR, et al. The  
797 JAK2/STAT3 signaling pathway is required for growth of CD44(+)CD24(-) stem cell-like  
798 breast cancer cells in human tumors. *J Clin Invest* 2011;121(7):2723-35.

799 41. Gao R, Li D, Xun J, Zhou W, Li J, Wang J, et al. CD44ICD promotes breast cancer stemness  
800 via PFKFB4-mediated glucose metabolism. *Theranostics* 2018;8(22):6248-62.

801 42. Giordano A, Gao H, Anfossi S, Cohen E, Mego M, Lee BN, et al. Epithelial-mesenchymal  
802 transition and stem cell markers in patients with HER2-positive metastatic breast  
803 cancer. *Mol Cancer Ther* 2012;11(11):2526-34.

804 43. Harrison H, Simoes BM, Rogerson L, Howell SJ, Landberg G, Clarke RB. Oestrogen  
805 increases the activity of oestrogen receptor negative breast cancer stem cells through  
806 paracrine EGFR and Notch signalling. *Breast Cancer Res* 2013;15(2):R21.

807 44. Joshi PA, Jackson HW, Beristain AG, Di Grappa MA, Mote PA, Clarke CL, et al.  
808 Progesterone induces adult mammary stem cell expansion. *Nature* 2010;465(7299):803-  
809 7.

810 45. Simoes BM, O'Brien CS, Eyre R, Silva A, Yu L, Sarmiento-Castro A, et al. Anti-estrogen  
811 Resistance in Human Breast Tumors Is Driven by JAG1-NOTCH4-Dependent Cancer Stem  
812 Cell Activity. *Cell Rep* 2015;12(12):1968-77.

813 46. Shea MP, O'Leary KA, Fakhraldeen SA, Goffin V, Friedl A, Wisinski KB, et al. Antiestrogen  
814 Therapy Increases Plasticity and Cancer Stemness of Prolactin-Induced ERalpha(+)  
815 Mammary Carcinomas. *Cancer Res* 2018;78(7):1672-84.

816 47. Daniel AR, Gaviglio AL, Knutson TP, Ostrander JH, D'Assoro AB, Ravindranathan P, et al.  
817 Progesterone receptor-B enhances estrogen responsiveness of breast cancer cells via  
818 scaffolding PELP1- and estrogen receptor-containing transcription complexes. *Oncogene*  
819 2015;34(4):506-15.

820 48. Rajaram RD, Buric D, Caikovski M, Ayyanan A, Rougemont J, Shan J, et al. Progesterone  
821 and Wnt4 control mammary stem cells via myoepithelial crosstalk. *EMBO J*  
822 2015;34(5):641-52.

823 49. Truong TH, Dwyer AR, Diep CH, Hu H, Hagen KM, Lange CA. Phosphorylated  
824 Progesterone Receptor Isoforms Mediate Opposing Stem Cell and Proliferative Breast  
825 Cancer Cell Fates. *Endocrinology* 2019;160(2):430-46.

826